NOAA Technical Memorandum ERL NSSL-92

MULTIPLE DOPPLER RADAR ANALYSIS OF SEVERE THUNDERSTORMS: DESIGNING A GENERAL ANALYSIS SYSTEM

R. A. Brown
C. R. Safford
S. P. Nelson
D. W. Burgess
W. C. Bumgarner
M. L. Weible
L. C. Fortner

Property of
NWC Library
University of Oklahoma

National Severe Storms Laboratory
Norman, Oklahoma
June 1981

UNITED STATES DEPARTMENT OF COMMERCE
Malcolm Baldrige, Secretary

NATIONAL OCEANIC AND ATMOSPHERIC ADMINISTRATION

Environmental Research Laboratories
Joseph O. Fletcher, Acting Director

TABLE OF CONTENTS

	Page
LIST OF FIGURES	iv
ABSTRACT	vi
1. INTRODUCTION	1
2. GENERAL FEATURES OF AN ANALYSIS SYSTEM	1
3. DATA CONSOLIDATION	1
4. DATA EDITING	3
4.1 Remaining Equipment Problems	3
4.2 Noisy Data	3
4.3 Side Lobe Problems	6
4.4 Range Aliasing of Radar Echoes	6
4.5 Doppler Velocity Aliasing	8
4.6 Ground Clutter Problems	11
4.7 Overall Editing Procedures	11
5. DATA INTERPOLATION TO A GRID ARRAY	12
5.1 Grid Array	12
5.2 Interpolation Procedures	14
6. SYNTHESIS OF MULTIPLE DOPPLER RADAR DATA	14
6.1 Data from Two Doppler Radars	14
6.2 Data from Three or More Doppler Radars	16
7. KINEMATIC ANALYSIS OF THREE DIMENSIONAL FLOW FIELD	17
8. DISPLAY OF DATA AND ANALYZED FIELDS	17
9. CONCLUDING COMMENTS	18
10. ACKNOWLEDGMENTS	18
11. REFERENCES	18

LIST OF FIGURES

Figure		Page
1	Flow diagram of the general multiple Doppler radar analysis system (enclosed within large box). Solid arrows indicate relationship of stages within the system. Dashed arrows indicate points at which other data can enter the system and points at which the output can be used for other purposes.	2
2	Flow diagram of the data editing stage.	4
3	Range-azimuth displays of (a) signal-to-noise ratios (dB) and (b) mean Doppler velocities (m s^{-1}) for the same constant elevation data locations prior to editing. Contour lines are for SNR values of 9.5 dB. Velocities with components away from the radar are positive. Data spacing in range is 0.6 km, azimuthal spacing is equivalent to about 0.6 km.	5
4	Relationship between range interval and mean Doppler velocity interval as a function of radar wavelength (λ). Dots indicate typical trade-offs between range and velocity intervals.	6
5	Schematic radar scope presentation of range ambiguity involving a WSW-ENE line of four radar echoes. Shaded echoes are those that actually would be detected by a Doppler radar having a limited range interval r_a.	7
6	Hypothetical Doppler velocity spectra illustrating the velocity aliasing problem at 3 and 10 cm wavelengths. The velocity interval lies between $-V_a$ and $+V_a$. Unshaded and shaded spectra represent all of the possible spectra within the ±100 m s^{-1} interval that could produce the measured (shaded) spectrum.	8
7	Range-azimuth presentation of aliased mean Doppler velocities. Hatched areas have SNR values less than 10 dB. Velocity values that are aliased (exceeding -35 m s^{-1}) are outlined by the thin lines. Maximum true value (at center of figure) is +7-70 = -63 m s^{-1} at a height of 13 km in a tornadic storm. Data spacing in range is 0.6 km, azimuthal spacing is equivalent to about 1.5 km.	9
8	Flow diagram of a Doppler velocity de-aliasing process (after having identified an aliased velocity). After de-aliasing, the new Doppler velocity value (V_r*) is set equal to A. However, if the aliased velocity can not be corrected, it is assumed that the velocity value really is not aliased. See the text for more discussion.	10
9	Exaggerated schematic of geometry used for computing horizontal (D) and vertical (z) distance of radar measurement (data point) from radar. See Eqs. (2) and (3).	13

Figure		Page
10	Example of flow field (synthesized from NSSL dual Doppler radar measurements) combined with University of Wyoming aircraft measurements (dashed flight path near 0.8 km height) on 8 June 1974. Reflectivity contours (thin solid lines) are in 10 dBZ intervals starting with 20 dBZ. Wind vector length (mean 1.3 km wind subtracted) equal to grid spacing is 10 m s^{-1}. Dark stippling indicates updraft and light stippling is downdraft. Thick solid lines show inflow-outflow boundaries. Circulation center (c) and surface tornado position (T) are indicated.	17

ABSTRACT

Synthesis and analysis of data acquired by multiple Doppler radars proceeds in stages of editing, data interpolation to grid points, synthesis of data for definition of three-dimensional flow, calculation of kinematic parameters, and display of analyzed data. We describe the procedure for designing such an analysis system. System design is based on many years of experience with NSSL's Multiple Radar Analysis (RADAN) System. A key feature of the system is its modular nature which permits individual components to be modified without affecting the rest of the system.

MULTIPLE DOPPLER RADAR ANALYSIS OF SEVERE THUNDERSTORMS: DESIGNING A GENERAL ANALYSIS SYSTEM

1. INTRODUCTION

During the past decade, Doppler radar has come to the forefront as an exciting meteorological research tool. A steady increase in the number of Doppler radars has led to a number of interagency cooperative field experiments utilizing multiple Doppler radar networks, such as the 1967, 1971, 1972, 1976 and 1977 Oklahoma field programs based at the National Severe Storms Laboratory (NSSL), the 1973, 1974 and 1976 National Hail Research Experiment (NHRE) in Colorado, the 1977 and 1978 Thunderstorm Research International Program (TRIP) in Florida and 1979 experiment in New Mexico, the 1978 Northern Illinois Meteorological Research On Downburst (NIMROD) experiment, the 1979 Severe Environmental Storms and Mesoscale Experiment (SESAME) in Oklahoma and the 1981 Cooperative Convective Precipitation Experiment (CCOPE) in Montana.

The attraction of multiple Doppler radar data is the capability of reconstructing three-dimensional flow fields. However, there are a number of steps involved between the collection of raw Doppler data and the synthesis of flow fields. This paper describes how to design an analysis system for producing meteorological information from the radar measurements. Most attention is devoted to system features that have not yet appeared in the literature. The discussion is based, in part, on what we have learned since 1973 using NSSL's Multiple Radar Analysis (RADAN) System.

2. GENERAL FEATURES OF AN ANALYSIS SYSTEM

An important consideration when designing an analysis system is to recognize that the system never will reach its "ultimate" configuration. There always will be unforeseen changes and refinements. Therefore, the design should have built-in flexibility.

One way to incorporate flexibility is to have a system consisting of modular units. Such a system is outlined in Fig. 1. In this example there are six stages involved from the reading of the basic radar data through the displaying of the final product: (1) the desired data are consolidated from the radar data tape, (2) erroneous data are deleted and aliased velocities are corrected, (3) data are interpolated to a three-dimensional grid array, (4) the three-dimensional wind field (u,v,w) is synthesized from multiple Doppler radar data, (5) kinematic fields are derived from u, v and w, and (6) data and analyzed fields are displayed. Each stage could consist of one or more computer programs. Details of each stage follow.

3. DATA CONSOLIDATION

Typically the researcher is interested in a subset of data on the radar data tape. Since the data can be reread several times during the editing stage, it is efficient to store the selected data subset in more compact form on a separate

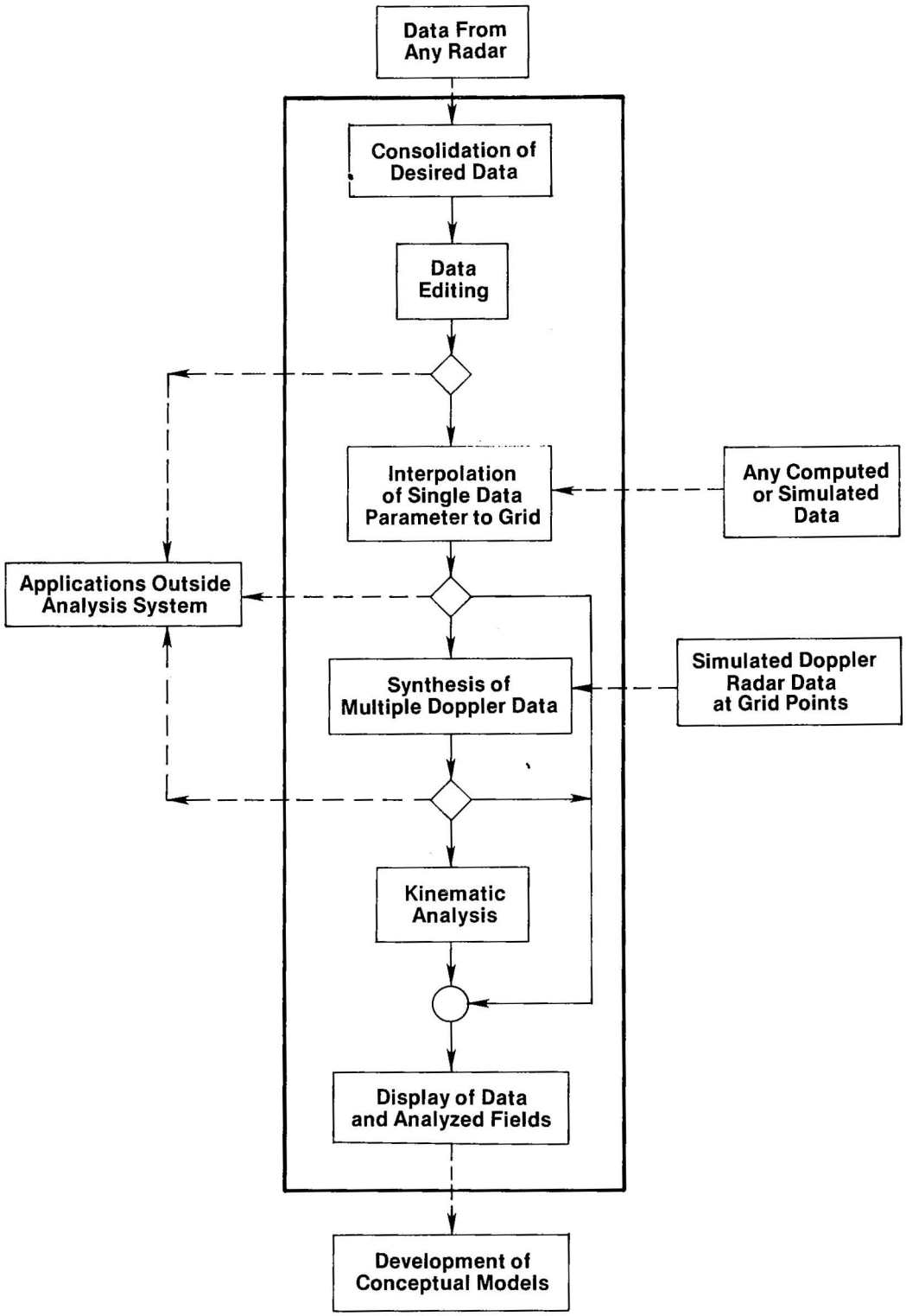

Figure 1. Flow diagram of the general multiple Doppler radar analysis system (enclosed within large box). Solid arrows indicate relationship of stages within the system. Dashed arrows indicate points at which other data can enter the system and points at which the output can be used for other purposes.

tape or on disk. Sometimes radar positioning information--such as azimuth, elevation, range, time--are erroneous (e.g., misalignment) or garbled and must be corrected before the data are consolidated. To aid further processing, the consolidated data format can be made independent of the individual radar input tape format.

4. DATA EDITING

The most critical--and time consuming--stage of the entire analysis system is data editing. Confirmation of the desired changes should be made by displaying the data after each set of corrections has been made. For this purpose, it is sufficient to present the data (reflectivity, mean Doppler velocity and Doppler spectrum width) in a range-azimuth format.

4.1 Remaining Equipment Problems

The data editing procedure is outlined in Fig. 2. The first step is to display all data points in order to find data problems and equipment malfunctions. Equipment problems span a wide range of obvious and subtle errors produced by equipment failures (e.g., Sirmans et al., 1977). After these problems have been corrected, attention is directed to the meteorological content of the data. There are several features that must be considered: noisy (bad) data, ground clutter and side lobe contamination, range aliasing obscuration and aliased Doppler velocity data.

4.2 Noisy Data

Within the finite sampling volume of a Doppler radar beam there are precipitation particles of various sizes moving in slightly different directions at differing speeds. The radar measures the electromagnetic field scattered from the ensemble of particles, which can be transformed into a Doppler velocity spectrum. The spectral mean provides an estimate of the reflectivity-weighted mean radial Doppler velocity component at that location within a storm. When the received power is weak, the signal-to-noise ratio (SNR) is small and therefore increased receiver noise makes it very difficult to compute a representative mean and width of the Doppler velocity spectrum.

Behavior of the mean velocity at low SNR is illustrated in Fig. 3. As the signal-to-noise ratio decreases, there is a marked increase in the variability of the velocity estimates (Sirmans and Bumgarner, 1975). By inspection one can choose a SNR value that will represent the threshold--or lowest value--for which the mean estimates seem reasonable. Note, however, that there can be some good velocity data on the "noisy" side of the threshold line and some bad values on the other side. This is one of the frustrations encountered while editing data. A reasonable compromise identifies a threshold value that excludes most of the noisy data.

After the computer program has deleted all data that have corresponding SNR values below the threshold level, the data can be displayed in range-azimuth format to see what problems remain. For the second editing step, all remaining bad data points can be identified (by azimuth, elevation and range position) and then deleted from the data field.

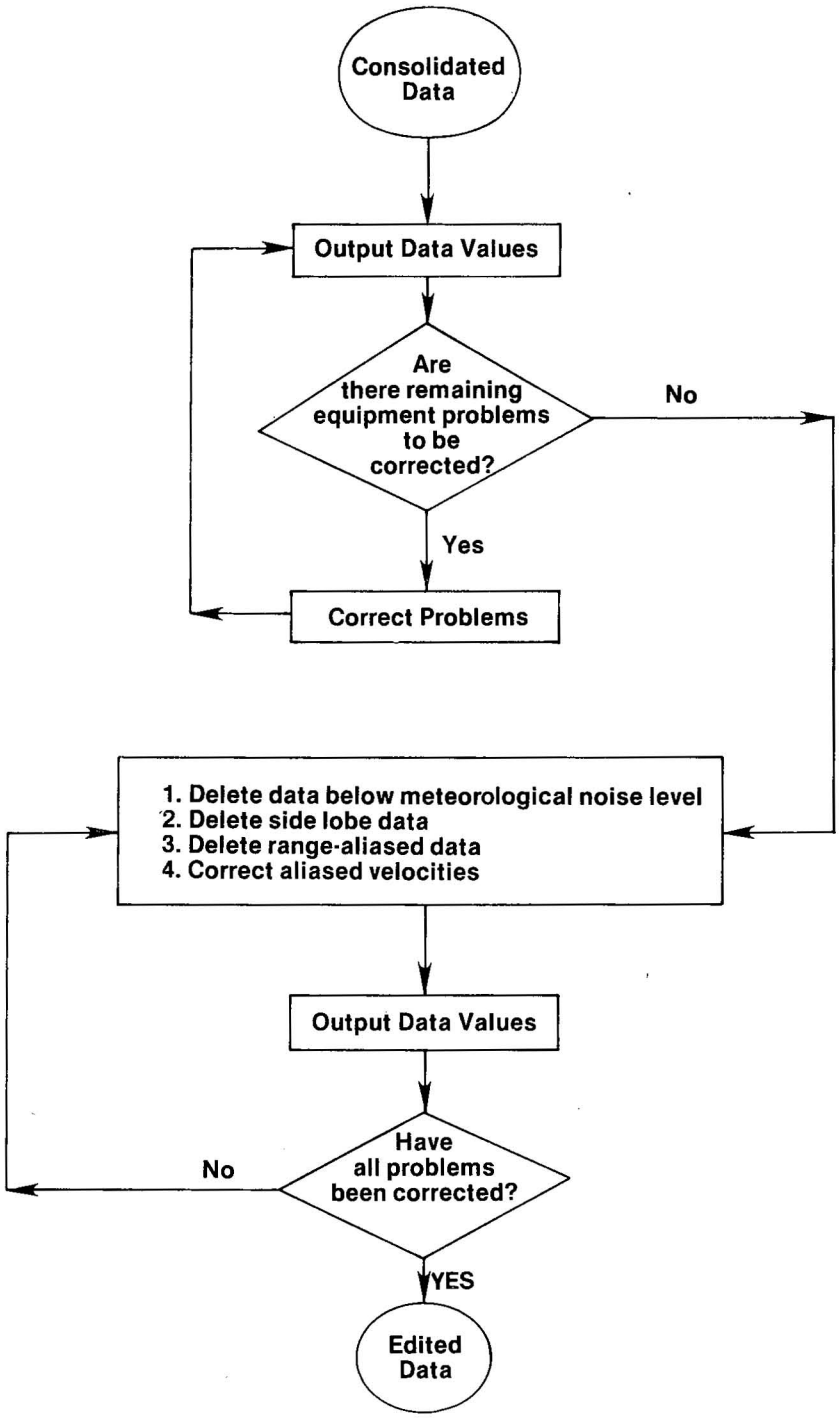

Figure 2. Flow diagram of the data editing stage.

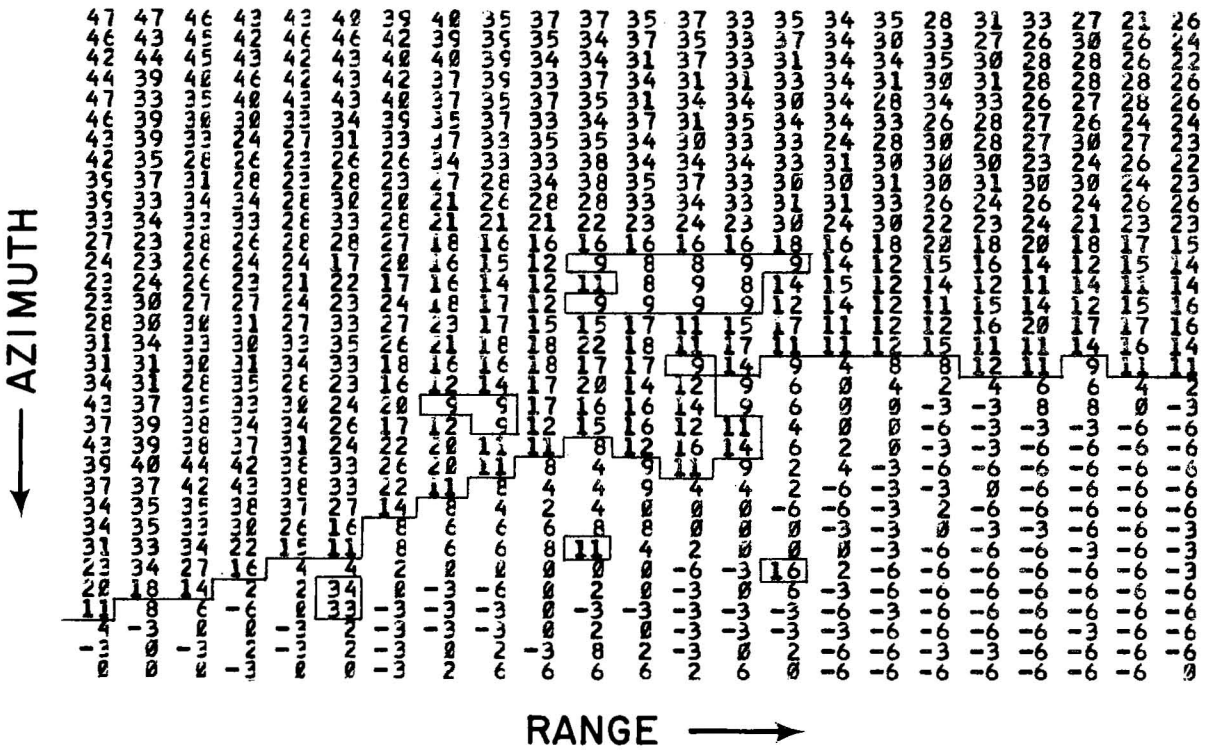

(a)

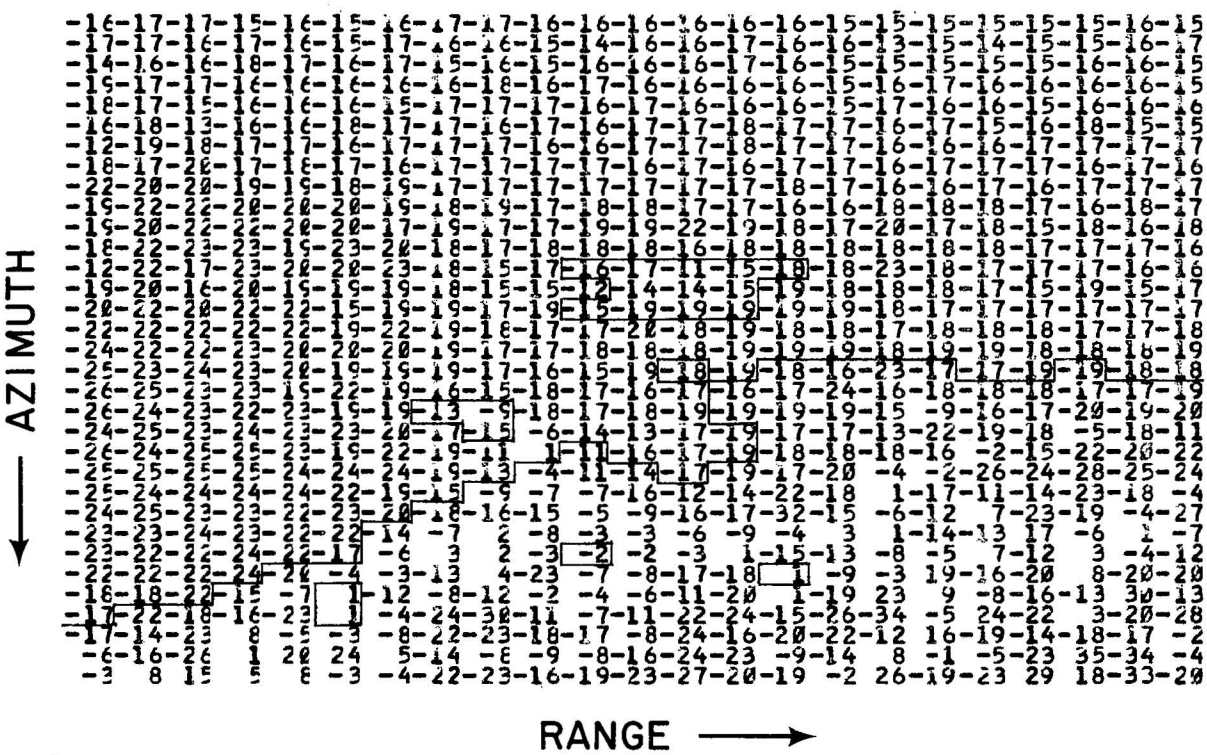

(b)

Figure 3. Range-azimuth displays of (a) signal-to-noise ratios (dB) and (b) mean Doppler velocities (m s^{-1}) for the same constant elevation data locations prior to editing. Contour lines are for SNR values of 9.5 dB. Velocities with components away from the radar are positive. Data spacing in range is 0.6 km, azimuthal spacing is equivalent to about 0.6 km.

4.3 Side Lobe Problems

When a radar scans through a severe storm, most of the returned power is received through the main lobe that is symmetric about the axis of a circular antenna. However, when the antenna (main lobe) is pointing just outside the radar echo it is possible for the weaker antenna side lobes to pick up enough return from adjacent 50 to 70 dBZ portions of the storm to exceed the SNR threshold; this is especially true when the threshold is set too low. In this situation, the radar echo will be wider or taller than it should be and Doppler velocity values will be positioned in areas that actually are outside the echo. (Battan, 1973, discusses the side lobe problem in greater detail.)

There are at least two ways in which fictitious side lobe echoes can be eliminated. One way is to select an appropriate SNR threshold level that is greater than the side lobe values. Side lob echoes often have large spectrum widths, so a second approach is to eliminate all data having associated width values greater than a critical value. In general, the use of a spectrum width cut-off value is advisable because the broader the Doppler velocity spectrum the less accurate is the mean Doppler velocity estimate.

4.4 Range Aliasing of Radar Echoes

The concept of aliasing is a characteristic of Doppler radar measurements that affects data collection and analysis. Thus, it can be shown (e.g., Battan, 1973) that the ambiguous (also called unambiguous) range interval (r_a) and maximum ambiguous (also called unambiguous) Doppler velocity (V_a) are interrelated in the following way:

$$V_a \cdot r_a = \lambda c/8 \qquad (1)$$

where λ is radar wavelength and c is radio propagation speed (3×10^8 m s^{-1}). The larger the desired range interval, the smaller is the velocity interval, and

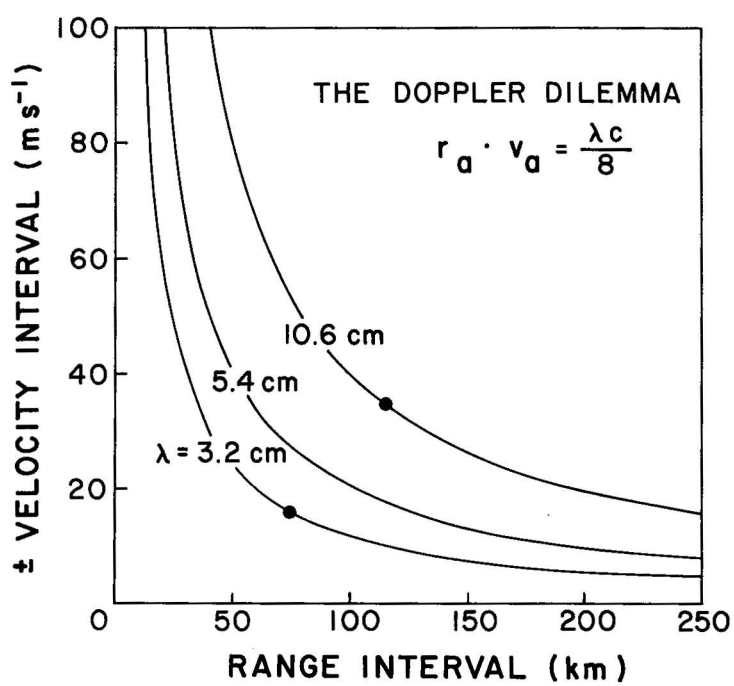

Figure 4. Relationship between range interval and mean Doppler velocity interval as a function of radar wavelength (λ). Dots indicate typical trade-offs between range and velocity intervals.

vice versa (Fig. 4). Therefore, a compromise must be found. Investigators using 3.2-cm wavelength Doppler radars typically choose a range interval of about 75 km and velocity interval of about 16 m s^{-1}--indicated by the dot in Fig. 4 (e.g., Lhermitte, 1970; Lhermitte, 1974).

For the study of severe storms, however, much larger velocity and range intervals are required. One then must use as long a wavelength as is practical, considering beamwidth and antenna size limitations. At 10-cm wavelengths, the compromise chosen for the NSSL Doppler radars is a range interval of 115 km and velocity interval of ±35 m s^{-1} (Brown et al., 1975). Another advantage of operation at this longer wavelength is reduced signal attenuation by heavy precipitation.

The range interval is the maximum distance (radial) at which a transmitted pulse can be scattered by precipitation and returned to the radar before the next pulse is transmitted. When a target is located beyond this range interval, the echo is received from that target after the next pulse is transmitted, and the echo signal is referenced by the radar to the most recent pulse. Thus, the echo appears on the PPI scope at an apparent range equal to the true range minus r_a (Fig. 5). Since the angular width of the echo area remains unchanged, the aliased echo usually appears elongated in the radial direction.

There are two editing problems associated with range aliasing. The simpler is that all the data are at the wrong range. This situation can be corrected by adding r_a to the range of each aliased data point. The solution is more complex when a "second-trip" echo (really between r_a and $2r_a$) is aliased on top of a "first-trip" echo. This situation is difficult to detect. However, there are a few clues: one portion (the second-trip portion) of an echo often appears to be elongated and out of place relative to the rest of the echo; or there is an unexpected region of large spectrum widths, representing the mixing of two different velocity fields. When range aliasing is suspected, it is wise to check radar echo locations on a radar having a range interval several times that of the Doppler radar. (Doviak et al. (1978) discuss a sophisticated real-time Doppler radar sampling scheme that detects range aliasing.)

In the editing process there is no automatic way to separate the two echoes. Typically the first-trip echo is the one of interest. If the second-trip echo is at least 10 to 15 dB weaker than the first-trip one, it contributes so little to the computation of the mean Doppler velocity value that it can be ignored (the

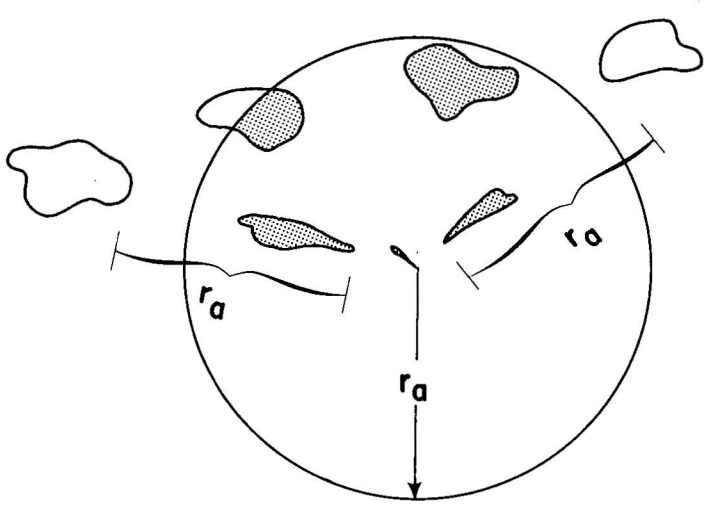

Figure 5. Schematic radar scope presentation of range ambiguity involving a WSW-ENE line of four radar echoes. Shaded echoes are those that actually would be detected by a Doppler radar having a limited range interval r_a.

DOPPLER RADAR RANGE AMBIGUITY

superimposed echo has to be considerably weaker not to affect spectrum width estimates). However, if the echoes have comparable received power, the data points that belong to the superimposed echoes must be deleted.

4.5 Doppler Velocity Aliasing

The measured Doppler velocity values may or may not represent the true values. If the true radial velocity exceeds the velocity limits of $\pm V_a$, the radar measures an erroneous (aliased) velocity value that lies within the $\pm V_a$ velocity interval and is offset from the true value by a multiple of $2V_a$ (Fig. 6). The mean of symmetric single-peaked spectra like those in Fig. 6 is equal to the value at the peak. Thus, a 3-cm Doppler radar having a velocity interval of ± 16 m s^{-1} measures a true spectrum mean velocity of 20 m s^{-1} as -12 m s^{-1} (20-32 m s^{-1}); in fact, true mean velocities of +52, +20, -12, -44 m s^{-1}, etc., all produce a measured mean Doppler velocity of -12 m s^{-1}. On the other hand, a 10-cm radar with ± 35 m s^{-1} velocity interval measures the true 20 m s^{-1} velocity correctly.

Looking at an individual Doppler velocity spectrum or mean of the spectrum, it is not possible to determine if velocity aliasing has taken place. However, if one looks at an entire two-dimensional field of mean Doppler velocity values, the aliased data points become obvious (Fig. 7). The characteristic that makes velocity aliasing so obvious is the abrupt change from $+V_a$ to $-V_a$, or vice versa, in a radial direction. (Abrupt changes in the azimuthal direction are not always due to aliasing; they could represent an unaliased tornadic vortex signature (Brown et al., 1978).)

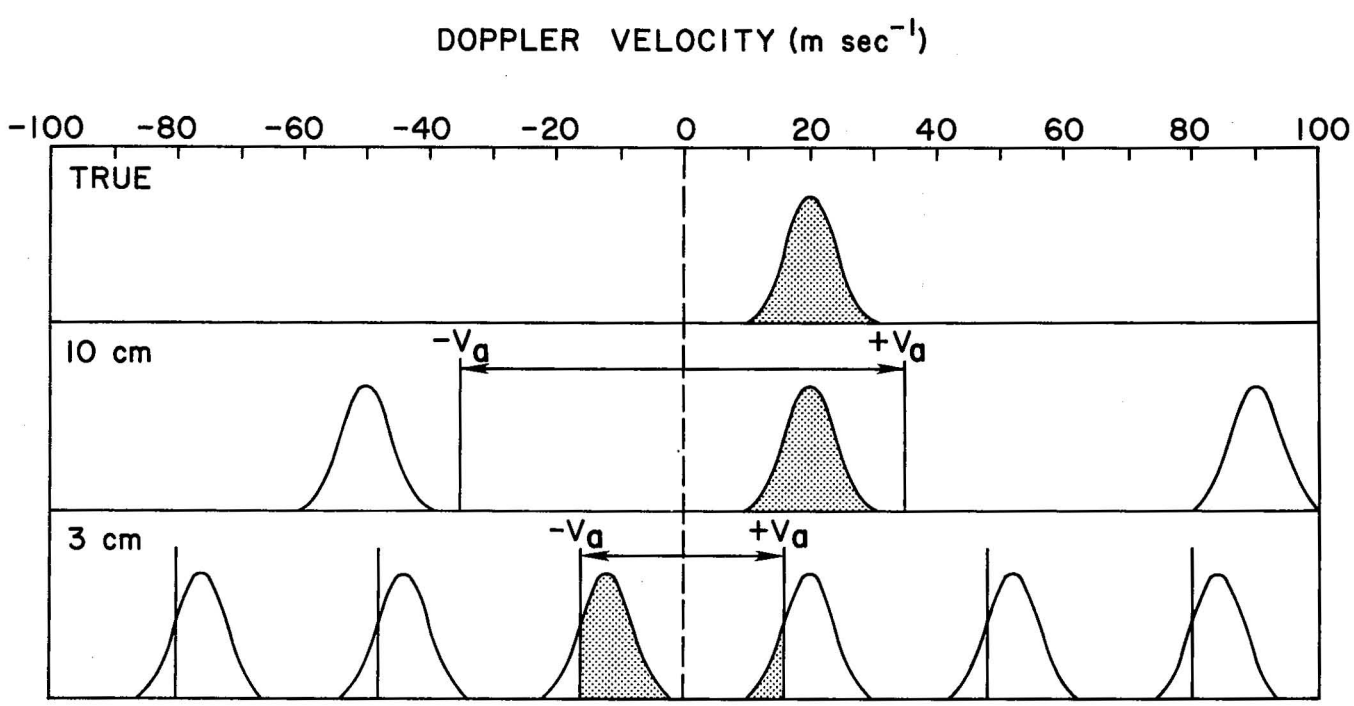

Figure 6. Hypothetical Doppler velocity spectra illustrating the velocity aliasing problem at 3 and 10 cm wavelengths. The velocity interval lies between $-V_a$ and $+V_a$. Unshaded and shaded spectra represent all of the possible spectra within the ± 100 m s^{-1} interval that could produce the measured (shaded) spectrum.

There are several approaches that can be used to de-alias Doppler velocity values. One technique is to take advantage of the abrupt velocity change with range. The procedure is to determine the Doppler velocity difference between one range location (V_r) and the previous range (V_{r-1}) by systematically progressing out each radial. If a velocity does not exist at the previous range location, the nearest value at a lesser range can be used. If there is no data point within a few kilometers, then the velocity value at the previous radial can be used. When the magnitude of the velocity difference exceeds a critical value (ΔV_c), the large difference is considered to be due to aliasing rather than to a natural velocity gradient; this technique fails when natural velocity differences approach or exceed $2V_a$.

In the simplest case, the proper Doppler velocity value is determined by adding $2V_a$ to V_r when V_r is negative or subtracting $2V_a$ when V_r is positive. For velocities that are aliased by an amount more than V_a, and especially $2V_a$, a more sophisticated procedure is required. The more sophisticated logic is outlined in Fig. 8. When velocities are aliased only once (N=1) but possibly by more than V_a, it is necessary to both add (S=+1) $2V_a$ to and subtract (S=-1) $2V_a$ from V_r. If the new value (A) decreases the velocity difference below the critical difference, then it is chosen as the proper de-aliased velocity (V_r*). However, if ΔV_c is still exceeded, a check is made for double aliasing (N=2) by adding $\pm 4V_a$ to V_r. The value of N is increased until the difference is less than ΔV_c. If N exceeds an arbitrary value of $125/V_a$ (no mean Doppler velocities in Oklahoma storms have

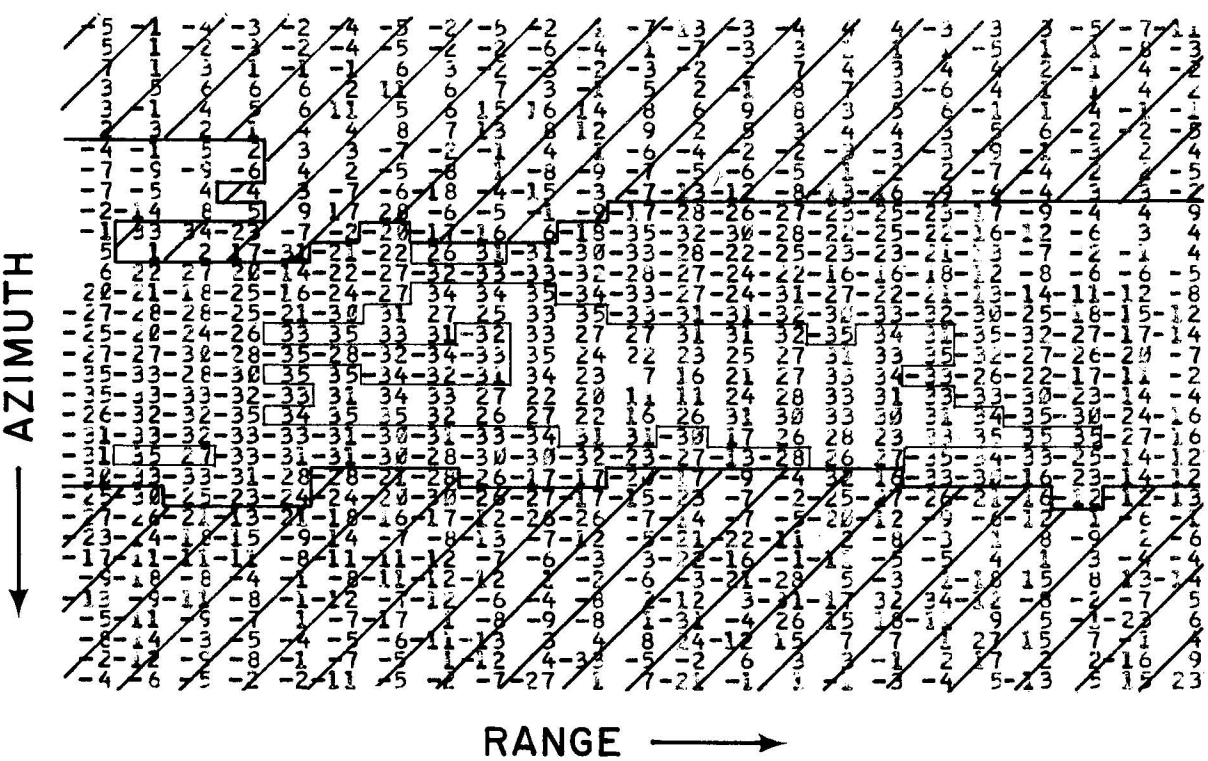

Figure 7. Range-azimuth presentation of aliased mean Doppler velocities. Hatched areas have SNR values less than 10 dB. Velocity values that are aliased (exceeding -35 m s^{-1}) are outlined by the thin lines. Maximum true value (at center of figure) is +7-70 = -63 m s^{-1} at a height of 13 km in a tornadic storm. Data spacing in range is 0.6 km, azimuthal spacing is equivalent to about 1.5 km.

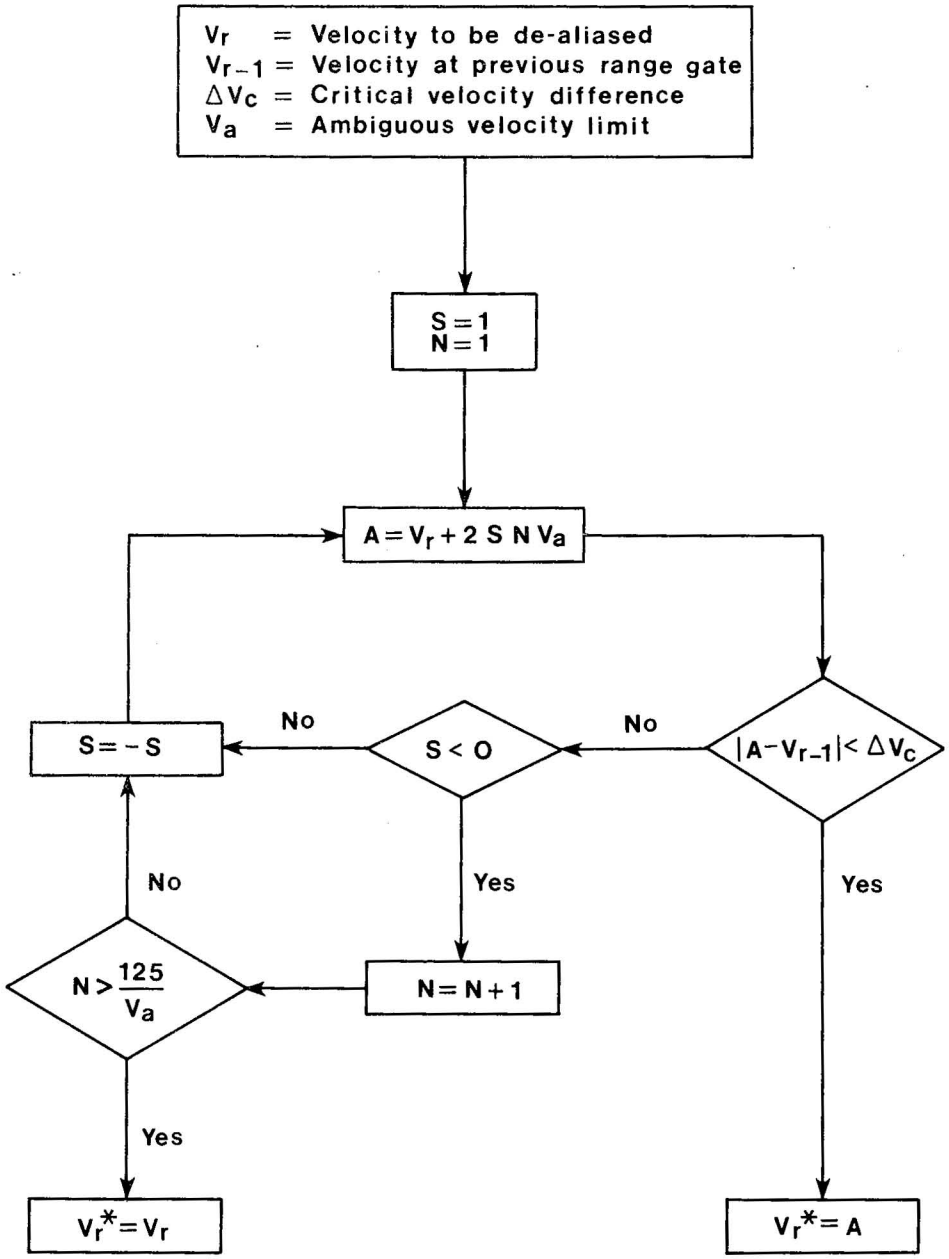

Figure 8. Flow diagram of a Doppler velocity de-aliasing process (after having identified an aliased velocity). After de-aliasing, the new Doppler velocity value (V_r) is set equal to A. However, if the aliased velocity can not be corrected, it is assumed that the velocity value really is not aliased. See the text for more discussion.*

exceeded ± 125 m s^{-1}) without satisfying the ΔV_c criteria, one may conclude that V_r is not aliased and should not have been identified as an aliased velocity in the first place.

Ray and Ziegler (1977) have proposed a different technique for de-aliasing Doppler velocities that easily can be incorporated into a general analysis system. Their approach is to construct a histogram of all Doppler velocities within a storm (or subregion). If the histogram contains both $+V_a$ and $-V_a$ (indicating that some velocities are aliased), a gap is searched for in the velocity distribution. The location of the gap is used to indicate which portion of the distribution represents aliased velocities. This procedure fails when velocities are found across the entire $2V_a$ interval; this may occur in severe storms especially with 3- and 5-cm wavelength Doppler radars.

4.6 Ground Clutter Problems

Radar return from ground targets (mean Doppler velocity equals zero) within a few tens of kilometers of a radar typically is strong enough to bias toward zero the mean velocity from a superimposed meteorological target. When the return is biased, the resulting reflectivity and Doppler velocity fields are characterized by marked variations from one data point to another. Yet some first-trip weather echoes may have reflectivity strong enough to overwhelm the weaker ground clutter areas.

The ground clutter pattern is repeated at the beginning of each multiple-trip range interval. Here the contamination problem becomes worse when a second-trip weather echo is at the same indicated range as the ground clutter because power (inversely proportional to the square of the distance to the target) received from a second-trip meteorological target is much weaker than the ground clutter.

There are at least two ways to approach the ground clutter problem. The first is via hardware: a ground clutter canceler, which is effectively a device to filter out signals with zero velocity, is added to the radar to significantly reduce the strength and areal extent of the ground target return. A second approach based on the same principle can be applied during the data collection process. If the radar collects data that can be transformed into a Doppler velocity spectrum, velocities near zero can be deleted from the spectrum before the mean Doppler velocity is calculated. Reflectivity values computed from the modified Doppler spectra also are less contaminated by ground clutter.

4.7 Overall Editing Procedures

In actual practice, the elimination of ground clutter, side-lobe data and data below a given threshold, the elimination of superimposed radar echoes and the correction of aliased Doppler velocity values all can be accomplished at the same time--after equipment problems have been corrected. Using the first range-azimuth display output, an optimum threshold SNR level can be determined by comparing the Doppler velocity, spectrum width and SNR values. Then the regions with ground return contamination and superimposed echoes can be identified (possibly using radar scope photographs). At the same time the critical velocity difference for de-aliasing Doppler velocity values can be determined by inspection. All of this information is fed into the editing program where bad data values are deleted radial by radial just before velocities are checked for aliasing.

A new range-azimuth display should be prepared to check the success of the first pass. If bad data still remain or some velocity values are not properly corrected, they can be taken care of during the next editing step. This process can be repeated (typically no more than one additional time) until only good Doppler velocity values remain in the edited data set.

At this point, it is possible that the edited data may be desired for a purpose external to this analysis system (indicated in Fig. 1). Some examples of such uses are for frequency distributions or other statistical studies (e.g., Doviak et al., 1978) and for developing real-time techniques for identification of single Doppler radar mesocyclone signatures in severe storms (e.g., Staff, NSSL et al., 1979).

5. DATA INTERPOLATION TO A GRID ARRAY

Since this analysis system is modular, edited data need not be the only data used in this stage. Any data field can be used as long as it has the same format as the edited data. One possible auxiliary data set could be simulated Doppler radar data. By inserting simulated data into the system at this point it is possible to confirm that the rest of the system is functioning properly. This approach is strongly recommended for checking out new, and even existing, multiple Doppler radar analysis systems.

In this stage, radar data are interpolated from a spherical array (range, azimuth, elevation) of data points to a common rectangular grid array that is independent of individual radar geometry and that represents a more suitable arrangement for analysis and interpretation.

5.1 Grid Array

When setting up a convenient three-dimensional grid array, one quickly encounters a predicament: data are collected relative to the earth's spherical surface but one would like the data to be presented relative to rectangular grid points.

Our approach is to use an orthogonal quasi-rectangular grid where each horizontal two-dimensional grid level is part of a spherical surface (concentric about the earth's center) and each vertical column of grid points is normal to the earth's surface (columns radiating outward from the earth's center). Data points from all radars can be interpolated precisely to these grid points. Then the entire grid can be deformed into an orthogonal rectangular grid by assuming that the horizontal grid levels are flat surfaces and that all vertical grid columns are parallel to each other.

The deformation results in negligible errors because of the limited horizontal (within 30 km of grid center) and vertical (15 to 20 km) extent of the grid relative to the earth's radius (6371 km). Vertical grid columns that are separated by 30 km at the earth's surface have been decreased from 30.09 km to 30.00 km separation at a height of 20 km. These differences are negligible when one remembers that radars have inherent data location uncertainties caused by their finite radar beamwidths (typically 0.5 km at ranges of 30 to 40 km) and pulse depths (typically 0.15 km). Over a distance of a few grid point intervals--where finite difference computations are made and where data are interpolated to grid locations--high-level distance errors caused by the deformation are found to be only a few meters.

Having provided an overview of this approach, details of some of the steps now are discussed. First, distance along the earth's surface and height above the surface are computed for each data point. The actual path traversed by a radar signal is determined by temperature and humidity variations along the beam and consequently the true path is not known. However, it commonly is assumed that the radar beam curves downward, but not by as much as the curvature of the earth's surface. Using the vertical profile of the index of refraction for the standard atmosphere, it can be shown that if the (spherical) earth's radius were increased by one-third, the curved path relative to the larger earth would be practically straight (e.g., Battan, 1973). This geometric simplification (Fig. 9) permits straight-forward computation of data point height (z) and distance on the earth (D) relative to the radar:

$$z = E[1 + (\frac{R}{E})^2 + \frac{2R}{E} \sin \phi]^{1/2} - E \qquad (2)$$

and

$$D = E \sin^{-1} [R \cos \phi/(E+z)] \qquad (3)$$

where R is slant range from radar to data point, ϕ is radar elevation angle and E is 1.33 times the sum of the earth's radius and radar height above sea level.

Next it is important to know where the grid origin--positioned at ground level in the middle of the data analysis area--is located relative to each radar. The range and azimuth of the origin can be specified from a reference radar. Then spherical trigonometry can be used to compute the origin's range and azimuth from the other radars.

Finally, the rectangular grid can be oriented relative to true north at the grid origin. The following three steps can be used to properly position each data point within the grid at a given reference time: (a) data point height above the

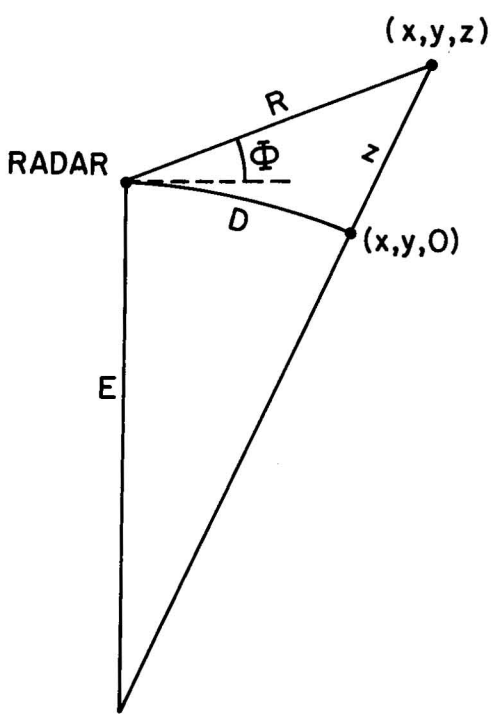

Figure 9. Exaggerated schematic of geometry used for computing horizontal (D) and vertical (z) distance of radar measurement (data point) from radar. See Eqs. (2) and (3).

radar can be determined using Eq. (2); (b) spherical trigonometry can be used to compute the data point's horizontal position relative to the grid origin; and (c) the horizontal position at an arbitrary reference time then can be determined by adjusting for the storm movement that took place between the reference time and the actual time of data collection (this step assumes that the storm is in a quasi-steady state during each three-dimensional volume scan).

5.2 Interpolation Procedures

Once data are positioned correctly relative to the quasi-rectangular grid points, the data values can be interpolated to the nearest grid points. There are a number of different interpolation procedures that have been employed for Doppler radar data; for example, bilinear interpolation (Miller and Strauch, 1974), Cressman weighting function (Brown, 1976), statistical weighting function (Heymsfield, 1976), exponential weighting function (Brandes, 1977), local polynomial fit (Ray et al., 1978). Most of them involve computing a weighted mean value from the surrounding data points. Again, the modular approach discussed here permits any of these procedures to be used or changed without affecting the rest of the system.

At this point in the analysis system, it is possible to proceed directly to the data display stage (Fig. 1). Some of the parameters that can be printed or contoured are reflectivity factor (from conventional or Doppler radar), mean Doppler radial velocity, spectrum width and auxiliary data (such as simulated data or computed shear values). Also the grid point data fields can be used as input for external purposes such as comparison of single Doppler velocity spectrum width values with aircraft turbulence (e.g., Lee, 1974).

6. SYNTHESIS OF MULTIPLE DOPPLER RADAR DATA

If data from two or more Doppler radars are to be synthesized into a three-dimensional wind field, the three previous stages (consolidation, editing and interpolation) must be repeated for data from each radar. It is advantageous to combine on one tape or on disk the interpolated Doppler velocity fields from each radar and the reflectivity factor data from one radar.

The synthesis process provides an estimate of the mean three-dimensional velocity of the precipitation particles in the radar sampling volume. A particle velocity is defined by three components of air motion (u,v,w) and its terminal fall velocity in still air (V_t). The objective is to solve for these four unknowns. Armijo (1969) has outlined the general procedure for doing this.

6.1 Data from Two Doppler Radars

For two radars, the Doppler velocity measurements (V_i) can be represented by

$$V_1 = \frac{1}{R_1} [x_1 u + y_1 v + z_1 (w + V_t)] \tag{4}$$

$$V_2 = \frac{1}{R_2} [x_2 u + y_2 v + z_2 (w + V_t)] \tag{5}$$

where R_i is the slant range from radar i to the data point location specified by

$$R_i = [x_i^2 + y_i^2 + z_i^2]^{1/2}$$

In Eqs. (4) and (5), Armijo assumed that the earth was flat; slant range really is relative to a curved earth's surface (Fig. 9). However, an error analysis reveals that slant range difference between a flat and curved earth is only 0.10% of the range at a height of 18 km and the difference decreases linearly to zero at the ground. So at a slant range of 100 km and height of 18 km, the slant range computed relative to the flat earth is in error by only 0.1 km. This type of error produces an uncertainty in the horizontal wind components that is much less than 0.1 m s^{-1}.

Whereas the geometry parameters (R_i, x_i, y_i, z_i) in Eqs. (4) and (5) are known, the four precipitation particle components are not known. With only two equations (one Doppler velocity measurement from each radar), the system is underdetermined. Therefore, two additional equations are required. As proposed by Armijo, they are the mass continuity equation and an assumed function for the terminal velocity. The continuity equation for a compressible atmosphere is

$$\frac{\partial u}{\partial x} + \frac{\partial v}{\partial y} + \frac{\partial w}{\partial z} = - \frac{w}{\rho}\frac{\partial \rho}{\partial z} \tag{6}$$

where ρ is air density. The derivation of Eq. (6) assumes that horizontal and temporal density variations are negligible compared to the terms remaining in (6). For terminal velocity, Rogers (1964) proposed V_t of raindrops to be a function of the equivalent radar reflectivity factor (Z_e)

$$V_t = -3.8 \left(\frac{\rho_o}{\rho}\right)^{0.4} Z_e^{0.0714} \tag{7}$$

where ρ is density at data height ($z+z_o$), ρ_o is sea level density and z_o is ground height above sea level; the density ratio factor is due to Foote and duToit (1969).

Armijo introduced the concept of synthesizing dual Doppler velocity data into air motion in a cylindrical coordinate system (symmetric about the radar baseline) and then transforming the motion field into a rectangular coordinate system. We are presenting an alternative procedure where the data are synthesized directly into a rectangular coordinate system; this procedure has been outlined by Brandes (1977a).

Using the set of equations (4)-(7), the three components of air motion (u,v,w) can be determined. First, from Eqs. (4) and (5), it can be shown that

$$u = A + B(w + V_t) \tag{8}$$

$$v = C + D(w + V_t) \tag{9}$$

where

$$A = (y_2R_1V_1 - y_1R_2V_2)/(x_1y_2 - x_2y_1)$$

$$B = (y_1z_2 - y_2z_1)/(x_1y_2 - x_2y_1)$$

$$C = R_1V_1/y_1 - Ax_1/y_1 \qquad C' = R_2V_2/y_2 - Ax_2/y_2$$

$$D = -Bx_1/y_1 - z_1/y_1 \qquad D' = -Bx_2/y_2 - z_2/y_2$$

(Note that when data are nearly east or west of radar 1, y_1 approaches zero and C and D become infinite; in this case C' and D' are used.) Equation (7) is used to eliminate V_t from Eqs. (8) and (9). The vertical velocity component at level 2 (w_2) can be computed from (6):

$$w_2 = w_1 - \overline{\left(\frac{w}{\rho}\frac{\partial \rho}{\partial z} + \frac{\partial u}{\partial x} + \frac{\partial v}{\partial y}\right)}\Delta z \qquad (10)$$

where w_2 is the vertical velocity at a vertical distance Δz from level 1 and the overbar represents the average of values at levels 1 and 2.

Note in Eqs. (8)-(10) that u, v and w are all functions of each other. Therefore, an iterative process must be used to determine the three components of motion. At the initial level, w is specified and u and v are computed based on that value. Then w_2 is estimated by assuming that u, v and w within the parentheses in Eq. (10) are the same at level 2 as at level 1. The w_2 estimate is used to estimate u and v at level 2. These values in turn are used to compute a new mean value within the parentheses of (10). This iterative process is continued until all u, v and w values at level 2 have become stabilized. (Defining stabilization as w differences of less than 0.01 m s^{-1} between consecutive iterations requires only three or four iterations on the average.)

6.2 Data from Three or More Doppler Radars

With three (or more) Doppler radars, there is a set of three (or more) equations of the general form

$$V_i = \frac{1}{R_i}\left[x_i u + y_i v + z_i(w + V_t)\right]$$

Armijo showed that u, v, and $(w+V_t)$ can be determined directly from the set of equations. He proposed that the equation of continuity be used to compute V_t, so that w can be separated from $(w+V_t)$. Experience has shown that $(w+V_t)$ becomes unstable when any of the radars has a low viewing angle (e.g., Miller, 1980; Nelson and Brown, 1981). Therefore, in most situations, a different procedure is required to separate w and V_t.

Vertical motion may be computed directly from u and v through use of the continuity equation. As is the case for dual Doppler synthesis, use of the continuity equation requires constraints at both the upper and lower limits of integration. Without constraints, vertical velocities in severe storms become unrealistically large due to the accumulation of small uncertainties in u and v (Ziegler, 1978; Nelson and Brown, 1981). It has been shown that the influence of u and v uncertainties is markedly less for downward integration when compared with upward integration (Bohne and Srivastava, 1975; Nelson and Brown, 1981).

Following the completion of the synthesis process, velocity fields can be placed on tape or disk for subsequent display or kinematic computations. The data also are available as input for research efforts that are external to the analysis system. For example, the data could be used to initialize models for retrieving temperature and pressure perturbations from wind fields (e.g., Bonesteele and Lin, 1978; Hane and Scott, 1978), to initialize models for determining precipitation trajectories within storms (e.g., Paluch, 1978; Ziegler, 1978; Nelson, 1980), to compare with numerical modeling results (e.g., Schlesinger, 1978; Wilhelmson and Klemp, 1978), or to help understand the initiation of lightning discharges in thunderstorms.

7. KINEMATIC ANALYSIS OF THREE-DIMENSIONAL FLOW FIELD

Having available a three-dimensional array of the flow field, there are a number of other quantities that could be computed. For example, velocity vectors, streamlines and isotachs could be constructed in either horizontal or vertical cross-sections. Vorticity and divergence fields also are important for understanding storm evolution (e.g., Ray, 1976; Heymsfield, 1978).

8. DISPLAY OF DATA AND ANALYZED FIELDS

At one stage in the analysis system one might like to display single Doppler radar parameters (reflectivity factor, mean Doppler velocity, width of Doppler velocity spectrum), while at another stage interest might be in the three components of air motion (u,v,w) and the terminal velocity component. At still another stage one may desire to see streamlines, isotachs or velocity vectors; or perhaps fields of divergence and vorticity.

Whatever the parameter, there are several different ways in which it can be displayed. The simplest output device is the printer. A more sophisticated and desirable device is the plotter or graphics display terminal. Computer system libraries usually have subroutines that make it easy to contour single parameter data fields, to plot two- or perhaps three-dimensional vector fields, and sometimes to draw streamlines of two-dimensional flow fields. It also is possible to present data in three-dimensional perspective.

The goal of an analysis system is to present the data and/or analyzed fields in forms that are most useful to the researcher. In the case of severe thunderstorm research, for example, products have been used for conventional radar studies of hailstorms (e.g., Nelson, 1977), for understanding mesocyclone evolution using single Doppler velocity data (e.g., Lemon et al., 1978), for understanding tornadogenesis relative to gust front (e.g., Brandes, 1977b) and mesocyclone evolution (e.g., Brandes, 1978) using multiple Doppler data, and for understanding the entire tornadic storm evolution through the use of aircraft and multiple Doppler radar measurements (e.g., Burgess et al., 1977; Fig. 10).

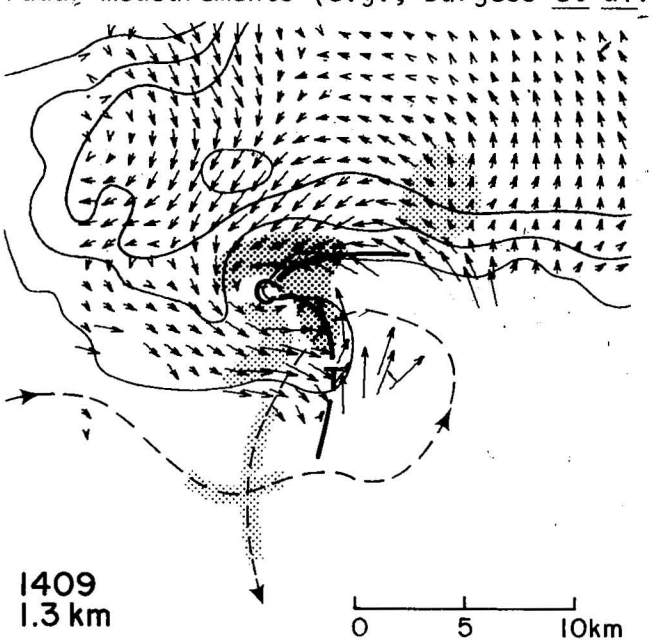

Figure 10. Example of flow field (synthesized from NSSL dual Doppler radar measurements) combined with University of Wyoming aircraft measurements (dashed flight path near 0.8 km height) on 8 June 1974. Reflectivity contours (thin solid lines) are in 10 dBZ intervals starting with 20 dBZ. Wind vector length (mean 1.3 km wind subtracted) equal to grid spacing is 10 m s^{-1}. Dark stippling indicates updraft and light stippling is downdraft. Thick solid lines show inflow-outflow boundaries. Circulation center (c) and surface tornado position (T) are indicated.

9. CONCLUDING COMMENTS

Factors to be considered in the design of a general multiple radar analysis system have been discussed. Several important aspects of such a system have been presented here for the first time.

One of the foremost considerations is data editing, where one must be on the lookout for a number of aliasing, equipment malfunction, and meteorologically-induced problems. Velocity aliasing is a universal problem encountered in the study of severe thunderstorms. We have outlined the de-aliasing algorithm used in the RADAN System. The algorithm has successfully identified mean Doppler velocity values in excess of 90 m s^{-1} (V_a = ±35 m s^{-1}).

Another critical consideration is the establishment of the three-dimensional grid to which the Doppler velocity measurements are interpolated. Spherical trigonometry must be employed to assure that the data from each radar are interpolated to the same points in space.

In general, an analysis system should be kept flexible so refinements, modifications, and updating can be accomplished with a minimum of effort. One way to incorporate flexibility is to design a system consisting of modular units. Our experience with the RADAN System indicates that this approach is viable, especially in light of many inevitable changes.

10. ACKNOWLEDGMENTS

The Doppler radar program at NSSL has been supported by funds of the National Oceanic and Atmospheric Administration, Department of Energy, Federal Aviation Administration and Nuclear Regulatory Commission. Discussions with Edward Brandes were very helpful during the development of the dual Doppler analysis technique presented here. Alice Adams, Richard Clark, James Hatten, Ross Hilbert, Brad Smull, and Vincent Wood provided valuable assistance with the development of the RADAN System. Sandra Mudd did her usual fine job in preparing the manuscript drafts. The graphics were ably prepared by Jennifer Moore, Joan Kimpel, and Charles Clark.

11. REFERENCES

Armijo, L., 1969: A theory for the determination of wind and precipitation velocities with Doppler radars. J. Atmos. Sci., 26, 570-573.

Battan, L. J., 1973: Radar Observation of the Atmosphere. Chicago, Univ. of Chicago Press, 324 pp.

Bohne, A. R., and R. C. Srivastava, 1975: Random errors in wind and precipitation fall speed measurements by a triple Doppler radar system. Lab. for Atmospheric Probing Tech. Rpt. No. 37, Univ. of Chicago, 44 pp.

Bonesteele, R. G., and Y. J. Lin, 1978: A study of updraft-downdraft interaction based on perturbation pressure and single-Doppler radar data. Mon. Wea. Rev., 106, 62-68.

Brandes, E. A., 1977a: Flow in severe thunderstorms observed by dual-Doppler radar. Mon. Wea. Rev., 105, 113-120.

_____, 1977b: Gust front evolution and tornado genesis as viewed by Doppler radar. J. Appl. Meteor., 16, 333-338.

_____, 1978: Mesocyclone evolution and tornadogenesis: some observations. Mon. Wea. Rev., 106, 995-1011.

Brown, R. A., 1976: Single Doppler radar data acquisition and analysis. Appendix E in The Union City, Oklahoma Tornado of 24 May 1973, R. A. Brown, Ed., NOAA Tech. Memo. ERL NSSL-80, Norman, Nat. Severe Storms Lab., 215-228 [NTIS PB269443/AS].

_____, L. R. Lemon and D. W. Burgess, 1978: Tornado detection by pulsed Doppler radar. Mon. Wea. Rev., 106, 29-38.

_____, D. W. Burgess, J. K. Carter, L. R. Lemon and D. Sirmans, 1975: NSSL dual-Doppler radar measurements in tornadic storms: a preview. Bull. Amer. Meteor. Soc., 56, 524-526.

Burgess, D. W., R. A. Brown, L. R. Lemon and C. R. Safford, 1977: Evolution of a tornadic thunderstorm. Preprints, 10th Conf. on Severe Local Storms, Boston, Amer. Meteor. Soc., 84-89.

Doviak, R. J., D. Sirmans, D. Zrnic and G. B. Walker, 1978: Considerations for pulse-Doppler radar observations of severe thunderstorms. J. Appl. Meteor., 17, 189-205.

Foote, G. B., and P. S. duToit, 1969: Terminal velocity of raindrops aloft. J. Appl. Meteor., 8, 249-253.

Hane, C. E., and B. C. Scott, 1978: Temperature and pressure perturbations within convective clouds derived from detailed air motion information: preliminary testing. Mon. Wea. Rev., 106, 654-661.

Heymsfield, G. M., 1976: Statistical objective analysis of dual-Doppler radar data from a tornadic storm. J. Appl. Meteor., 15, 59-68.

_____, 1978: Kinematic and dynamic aspects of the Harrah tornadic storm analyzed from dual-Doppler radar data. Mon. Wea. Rev., 106, 233-254.

Lee, J. T., 1974: Thunderstorm turbulence concurrent Doppler radar and aircraft observations 1973. Preprints, 6th Conf. on Aerospace and Aeron. Meteor., Boston, Amer. Meteor. Soc., 295-298.

Lemon, L. R., D. W. Burgess and R. A. Brown, 1978: Tornadic storm airflow and morphology derived from single-Doppler radar measurements. Mon. Wea. Rev., 106, 48-61.

Lhermitte, R. M., 1970: Dual-Doppler radar observation of convective storm circulation. Preprints, 14th Radar Meteor. Conf., Boston, Amer. Meteor. Soc., 139-144.

_____, 1974: Dual Doppler radar study of south Florida convective storms. Preprints, Conf. on Cloud Physics, Boston, Amer. Meteor. Soc., 328-332.

Miller, L. J., 1980: Dynamical-microphysical evolution of a convective storm. Part II: Airflow from multiple Doppler observations. NCAR Tech. Note 151+STR, Boulder, Natl. Center for Atmos. Res., 68-120.

_____ and R. G. Strauch, 1974: A dual Doppler radar method for the determination of wind velocities within precipitating weather systems. Remote Sensing of Environ., 3, 219-235.

Nelson, S. P., 1977: Rear flank downdraft: a hailstorm intensification mechanism. Preprints, 10th Conf. on Severe Local Storms, Boston, Amer. Meteor. Soc., 521-525.

_____, 1980: Hail production in a supercell-type storm. Preprints, Third WMO Conf. on Weather Modification, Clermont-Ferrand, France.

_____ and R. A. Brown, 1981: Multiple Doppler radar derived vertical velocities in thunderstorms: Error analysis and solution techniques. To be submitted to J. Appl. Meteor.

Paluch, I. R., 1978: Size sorting of hail in a three-dimensional updraft and implications for hail suppression. J. Appl. Meteor., 17, 763-777.

Ray, P. S., 1976: Vorticity and divergence fields within tornadic storms from dual-Doppler observations. J. Appl. Meteor., 15, 879-890.

___, and C. L. Ziegler, 1977: De-aliasing first-moment Doppler estimates. J. Appl. Meteor., 16, 563-564.

___, K. K. Wagner, K. W. Johnson, J. J. Stephens, W. C. Bumgarner and E. A. Mueller, 1978: Triple-Doppler observations of a convective storm. J. Appl. Meteor., 17, 1202-1212.

Rogers, R. R., 1964: An extension of the Z-R relation for Doppler radar. Preprints, 11th Weather Radar Conf., Boston, Amer. Meteor. Soc., 158-161.

Schlesinger, R. E., 1978: A three-dimensional numerical model of an isolated thunderstorm: Part I. Comparative experiments for variable ambient wind shear. J. Atmos. Sci., 35, 690-713.

Sirmans, D., and B. Bumgarner, 1975: Numerical comparison of five mean frequency estimators. J. Appl. Meteor., 14, 991-1003.

_____, J. Dooley and B. Bumgarner, 1977: Spring program '76, Section II: Doppler radar data quality control summary. NOAA Tech. Memo. ERL NSSL-83, Norman, Nat. Severe Storms Lab., 77-130. [NTIS PB280745/AS]

Staff, National Severe Storms Lab., Air Force Geophysics Lab., National Weather Service and Air Weather Service, 1979: Final report on the Joint Doppler Operational Project (JDOP) 1976-78. NOAA Tech. Memo. ERL NSSL-86, Norman, Nat. Severe Storms Lab., 84 pp.

Wilhelmson, R. B., and J. B. Klemp, 1978: A numerical study of storm splitting that leads to long-lived storms. J. Atmos. Sci., 35, 1974-1986.

Ziegler, C. L., 1978: A dual Doppler variational objective analysis as applied to studies of convective storms. NOAA Tech. Memo. ERL NSSL-85, Norman, Nat. Severe Storms Lab., 116 pp. [NTIS PB293581/AS]

NATIONAL SEVERE STORMS LABORATORY

The NSSL Technical Memorandum, beginning with No. 28, continue the sequence established by the U. S. Weather Bureau National Severe Storms Project, Kansas City, Missouri. Numbers 1-22 were designated NSSP Reports. Numbers 23-27 were NSSL Reports, and 24-27 appeared as subseries of Weather Bureau Technical Notes. These reports are available from the National Technical Information Service, Operations Division, Springfield, Virginia 22151, a microfiche version for $3.50 or a hard copy, cost depending upon the number of pages. NTIS numbers are given below in parenthesis.

No. 1 National Severe Storms Project Objectives and Basic Design. Staff, NSSP. March 1961, 16 p. (PB-168207)

No. 2 The Development of Aircraft Investigations of Squall Lines from 1956-1960. B. B. Goddard. 34 p. (PB-168208)

No. 3 Instability Lines and Their Environments as Shown by Aircraft Soundings and Quasi-Horizontal Traverses. D. T. Williams. February 1962. 15 p. (PB-168209)

No. 4 On the Mechanics of the Tornado. J. R. Fulks. February 1962. 33 p. (PB-168210)

No. 5 A Summary of Field Operations and Data Collection by the National Severe Storms Project in Spring 1961. J. T. Lee. March 1962. 47 p. (PB-165095)

No. 6 Index to the NSSP Surface Network. T. Fujita. April 1962. 32 p. (PB-168212)

No. 7 The vertical structure of Three Dry Lines as Revealed by Aircraft Traverses. E. L. McGuire. April 1962. 10 p. (PB-168213)

No. 8 Radar Observations of a Tornado Thunderstorm in Vertical Section. Ralph J. Donaldson, Jr. April 1962. 21 p. (PB-174859)

No. 9 Dynamics of Severe Convective Storms. Chester W. Newton. July 1962. 44 p. (PB-163319)

No. 10 Some Measured Characteristics of Severe Storms Turbulence. Roy Steiner and Richard H. Rhyne. July 1962. 17 p. (N62-16401)

No. 11 A Study of the Kinematic Properties of Certain Small-Scale Systems. D. T. Williams. October 1962. 22 p. (PB-168216)

No. 12 Analysis of the Severe Weather Factor in Automatic Control of Air Route Traffic. W. Boynton Beckwith. December 1962. 67 p. (PB-168217)

No. 13 500-Kc./Sec. Sferics Studies in Severe Storms. Douglas A. Kohl and John E. Miller. April 1963. 36 p. (PB-168218)

No. 14 Field Operations of the National Severe Storms Project in Spring 1962. L. D. Sanders. May 1963. 71 p. (PB-168219)

No. 15 Penetrations of Thunderstorms by an Aircraft Flying at Supersonic Speeds. G. P. Roys. Radar Photographs and Gust Loads in Three Storms of 1961 Rough Rider. Paul W. J. Schumacher. May 1963. 19 p. (PB-168220)

No. 16 Analysis of Selected Aircraft Data from NSSP Operations, 1962. T. Fujita. May 1963. 29 p. (PB-168221)

No. 17 Analysis of Methods for Small-Scale Surface Network Data. D. T. Williams. August 1963. 20 p. (PB-168222)

No. 18 The Thunderstorm Wake of May 4, 1961. D. T. Williams. August 1963. 23 p. (PB-168223)

No. 19 Measurements by Aircraft of Condensed Water in Great Plains Thunderstorms. George P. Roys and Edwin Kessler. July 1966. 17 p. (PB-173048)

No. 20 Field Operations of the National Severe Storms Project in Spring 1963. J. T. Lee, L. D. Sanders, and D. T. Williams. January 1964. 68 p. (PB-168224)

No. 21 On the Motion and Predictability of Convective Systems as Related to the Upper Winds in a Case of Small Turning of Wind with Height. James C. Fankhauser. January 1964. 36 p. (PB-168225)

No. 22 Movement and Development Patterns of Convective Storms and Forecasting the Probability of Storm Passage at a Given Location. Chester W. Newton and James C. Fankhauser. January 1964. 53 p. (PB-168226)

No. 23 Purposes and Programs of the National Severe Storms Laboratory, Norman, Oklahoma. Edwin Kessle December 1964. 17 p. (PB-166675)

No. 24 Papers on Weather Radar, Atmospheric Turbulence, Sferics and Data Processing. August 1965. 139 p. (AD-621586)

No. 25 A Comparison of Kinematically Computed Precipitation with Observed Convective Rainfall. James C. Fankhauser. September 1965. 28 p. (PB-168445)

No. 26 Probing Air Motion by Doppler Analysis of Radar Clear Air Returns. Roger M. Lhermitte. May 1966. 37 p. (PB-170636)

No. 27 Statistical Properties of Radar Echo Patterns and the Radar Echo Process. Larry Armijo. May 1966. The Role of the Kutta-Joukowski Force in Cloud Systems with Circulation. J. L. Goldman. May 1966. 34 p. (PB-170756)

No. 28 Movement and Predictability of Radar Echoes. James Warren Wilson. November 1966. 30 p. (PB-173972)

No. 29 Notes on Thunderstorm Motions, Heights, and Circulations. T. W. Harrold, W. T. Roach, and Kenneth E. Wilk. November 1966. 51 p. (AD-644899)

No. 30 Turbulence in Clear Air Near Thunderstorms. Anne Burns, Terence W. Harrold, Jack Burnham, and Clifford S. Spavins. December 1966. 20 p. (PB-173992)

No. 31 Study of a Left-Moving Thunderstorm of 23 April 1964. George R. Hammond. April 1967. 75 p. (PB-174681)

No. 32 Thunderstorm Circulations and Turbulence from Aircraft and Radar Data. James C. Fankhauser and J. T. Lee. April 1967. 32 p. (PB-174860)

No. 33 On the Continuity of Water Substance. Edwin Kessler. April 1967. 125 p. (PB-175840)

No. 34 Note on the Probing Balloon Motion by Doppler Radar. Roger M. Lhermitte. July 1967. 14 p. (PB-175930)

No. 35 A Theory for the Determination of Wind and Precipitation Velocities with Doppler Radars. Larry Armijo. August 1967. 20 p. (PB-176376)

No. 36 A Preliminary Evaluation of the F-100 Rough Rider Turbulence Measurement System. U. O. Lappe. October 1967. 25 p. (PB-177037)

No. 37 Preliminary Quantitative Analysis of Airborne Weather Radar. Lester P. Merritt. December 1967. 32 p. (PB-177188)

No. 38 On the Source of Thunderstorm Rotation. Stanley L. Barnes. March 1968. 28 p. (PB-178990)

No. 39 Thunderstorm - Environment Interactions Revealed by Chaff Trajectories in the Mid-Troposphere. James C. Fankhauser. June 1968. 14 p. (PB-179659)

No. 40 Objective Detection and Correction of Errors in Radiosonde Data. Rex L. Inman. June 1968. 50 p. (PB-180284)

No. 41 Structure and Movement of the Severe Thunderstorms of 3 April 1964 as Revealed from Radar and Surface Mesonetwork Data Analysis. Jess Charba and Yoshikazu Sasaki. October 1968. 47 p. (PB-183310)

No. 42 A Rainfall Rate Sensor. Brian E. Morgan. November 1968. 10 p. (PB-183979)

No. 43 Detection and Presentation of Severe Thunderstorms by Airborne and Ground-based Radars: A Comprehensive Study. Kenneth E. Wilk, John K. Carter, and J. T. Dooley. February 1969. 56 p. (PB-183572)

No. 44 A Study of a Severe Local Storm of 16 April 1967. George Thomas Haglund. May 1969. 54 p. (PB-184970)

No. 45 On the Relationship Between Horizontal Moisture Convergence and Convective Cloud Formation. Horace R. Hudson. March 1970. 29 p. (PB-191720)

No. 46 Severe Thunderstorm Radar Echo Motion and Related Weather Events Hazardous to Aviation Operations. Peter A. Barclay and Kenneth E. Wilk. June 1970. 63 p. (PB-192498)

No. 47 Evaluation of Roughness Lengths at the NSSL-WKY Meteorological Tower. Leslie D. Sanders and Allen H. Weber. August 1970. 24 p. (PB-194587)

No. 48 Behavior of Winds in the Lowest 1500 ft in Central Oklahoma: June 1966-May 1967. Kenneth C. Crawford and Horace R. Hudson. August 1970. 57 p. (N71-10615)

No. 49 Tornado Incidence Maps. Arnold Court. August 1970. 76 p. (COM-71-00019)

No. 50 The Meteorologically Instrumented WKY-TV Tower Facility. John K. Carter. September 1970. 18 p. (COM-71-00108)

No. 51 Papers on Operational Objective Analysis Schemes at the National Severe Storms Forecast Center. Rex L. Inman. November 1970. 91 p. (COM-71-00136)

No. 52 The Exploration of Certain Features of Tornado Dynamics Using a Laboratory Model. Neil B. Ward. November 1970. 22 p. (COM-71-00139)

No. 53 Rawinsonde Observation and Processing Techniques at the National Severe Storms Laboratory. Stanley L. Barnes, James H. Henderson and Robert J. Ketchum. April 1971. 245 p. (COM-71-00707)

No. 54 Model of Precipitation and Vertical Air Currents. Edwin Kessler and William C. Bumgarner. June 1971. 93 p. (COM-71-00911)

No. 55 The NSSL Surface Network and Observations of Hazardous Wind Gusts. Operations Staff. June 1971. 20 p. (COM-71-00910)

No. 56 Pilot Chaff Project at the National Severe Storms Laboratory. Edward A. Jessup. November 1971. 36 p. (COM-72-10106)

No. 57 Numerical Simulation of Convective Vortices. Robert P. Davies-Jones and Glenn T. Vickers. November 1971. 27 p. (COM-72-10269)

No. 58 The Thermal Structure of the Lowest Half Kilometer in Central Oklahoma: December 9, 1966-May 31, 1967. R. Craig Goff and Horace R. Hudson. July 1972. 53 p. (COM-72-11281)

No. 59 Cloud-to-Ground Lightning Versus Radar Reflectivity in Oklahoma Thunderstorms. Gilbert D. Kinzer. September 1972. 24 p. (COM-73-10050)

No. 60 Simulated Real Time Displays of Velocity Fields by Doppler Radar. L. D. Hennington and G. B. Walker. November 1972. 10 p. (COM-73-10515)

No. 61 Gravity Current Model Applied to Analysis of Squall-Line Gust Front. Jess Charba. November 1972. 58 p. (COM-73-10410)

No. 62 Mesoscale Objective Map Analysis Using Weighted Time-Series Observations. Stanley L. Barnes. March 1973. 60 p. (COM-73-10781)

No. 63 Observations of Severe Storms on 26 and 28 April 1971. Charles L. Vlcek. April 1973. 19 p. (COM-73-11200)

No. 64 Meteorological Radar Signal Intensity Estimation. Dale Sirmans and R. J. Doviak. September 1973. 80 p. (COM-73-11923/2AS)

No. 65 Radisonde Altitude Measurement Using Double Radiotheodolite Techniques. Stephan P. Nelson. September 1973. 20 p. (COM-73-11932/9AS)

No. 66 The Motion and Morphology of the Dryline. Joseph T. Schaefer. September 1973. 81 p. (COM-74-10043)

No. 67 Radar Rainfall Pattern Optimizing Technique. Edward A. Brandes. March 1974. 16 p. (COM-74-10906/AS)

No. 68 The NSSL/WKY-TV Tower Data Collection Program: April-July 1972. R. Craig Goff and W. David Zittel. May 1974. 45 p. (COM-74-11334/AS)

No. 69 Papers on Oklahoma Thunderstorms, April 29-30, 1970. Stanley L. Barnes, Editor. May 1974. 147 p. (COM-74-11474/AS)

No. 70 Life Cycle of Florida Key's Waterspouts. Joseph H. Golden. June 1974. 147 p. (COM-74-11477/AS)

No. 71 **Interaction of Two Convective Scales Within a Severe Thunderstorm: A Case Study and Thunderstorm** Wake Vortex Structure and Aerodynamic Origin. Leslie R. Lemon. June 1974. 43 p. (COM-74-11642/AS)

No. 72 Updraft Properties Deduced from Rawinsoundings. Robert P. Davies-Jones and James H. Henderson. October 1974. 117 p. (COM-75-10583/AS)

No. 73 Severe Rainstorm at Enid, Oklahoma - October 10, 1973. L. P. Merritt, K. E. Wilk, and M. L. Weible. November 1974. 50 p. (COM-75-10583/AS)

No. 74 Mesonetwork Array: Its Effect on Thunderstorm Flow Resolution. Stanley L. Barnes. October 1974. 16 p. (COM-75-10248/AS)

No. 75 Thunderstorm-Outflow Kinematics and Dynamics. R. Craig Goff. December 1975. 63 p. (PB-250808/AS)

No. 76 An Analysis of Weather Spectra Variance in a Tornadic Storm. Philippe Waldteufel. May 1976. 80 p. (PB-258456/AS)

No. 77 Normalized Indices of Destruction and Deaths by Tornadoes. Edwin Kessler and J. T. Lee. June 1976. 47 p. (PB-260923/AS)

No. 78 Objectives and Accomplishments of the NSSL 1975 Spring Program. K. Wilk, K. Gray, C. Clark, D. Sirmans, J. Dooley, J. Carter, and W. Bumgarner. July 1976. 47 p. (PB-263813/AS)

No. 79 Subsynoptic Scale Dynamics As Revealed By The Use Of Filtered Surface Data. Charles A. Doswell III. December 1976. 40 p. (PB-265433/AS)

No. 80 The Union City, Oklahoma Tornado of 24 May 1973. Rodger A. Brown, Editor. December 1976. 235 p. (PB-269443/AS)

No. 81 Mesocyclone Evolution and Tornado Generation Within the Harrah, Oklahoma Storm. Edward A. Brandes. May 1977 28 p. (PB-271675/AS)

No. 82 The Tornado: An Engineering-Oriented Perspective. Joseph E. Minor, James R. McDonald, and Kishor C. Mehta. December 1977. 196 p. (PB-281860/AS)

No. 83 Spring Program '76. R. L. Alberty, J. F. Weaver, D. Sirmans, J. T. Dooley, and B. Bumgarner. December 1977. 130 p. (PB280745/AS)

No. 84 Spring Program '77. P. S. Ray, J. Weaver, and NSSL Staff. December 1977. 173 p. (PB-284953/AS)

No. 85 A Dual-Doppler Variational Objective Analysis as Applied to Studies of Convective Storms. Conrad L. Ziegler. November 1978. 116 p. (PB-293581/AS)

No. 86 Final Report on the Joint Doppler Operational Project (JDOP) 1976-78. Prepared by Staff of the National Severe Storms Laboratory, Environmental Research Laboratories; Weather Radar Branch, Air Force Geophysics Laboratory; Equipment Development Laboratory, National Weather Service; and Air Weather Service, United States Air Force. March 1979. 84 p. (PB80-107188/AS)

No. 87 An Analysis of the Clear Air Planetary Boundary Layer Wind Synthesized from NSSL's Dual Doppler-Radar Data. Myron I. Berger and R. J. Doviak. June 1979. 55 p. (PB-300865/AS)

No. 88 The Relationship of the 300-mb Jet Stream to Tornado Occurrence. Carolyn M. Kloth and Robert P. Davies-Jones. July 1980. 62 p.

No. 89 A Study of Hail Production in a Supercell Storm Using a Doppler Derived Wind Field and a Numerical Hail Growth Model. Stephan P. Nelson. December 1980. 90 p. (PB81-178220)

No. 90 Summary of AEC-ERDA-NRC Supported Research at NSSL 1973-1979. J. T. Lee, Dusan Zrnic', Robert Davies-Jones and Joseph H. Golden. March 1981. 93 p.

No. 91 1980 Spring Program Summary. R. J. Doviak, Editor. April 1981. 128 p.